Electrolytic seawater mineralization and how it ensures (net) carbon dioxide removal

Erika Callagon La Plante,[1,2,3,4,] Xin Chen,[2,4,5] Steven Bustillos,[2,5,6] Arnaud Bouissonnie,[2,5] Thomas Traynor,[2,4] David Jassby,[2,4,5] Lorenzo Corsini,[4] Dante Simonetti,[2,4,6] and Gaurav Sant[2,4,5,7,8,*]*

[1] Department of Materials Science and Engineering, University of Texas at Arlington, Arlington, TX
[2] Institute for Carbon Management, University of California, Los Angeles, Los Angeles, CA
[3] Center for Advanced Construction Materials, University of Texas at Arlington, Arlington, TX
[4] Equatic Inc., Los Angeles, CA
[5] Department of Civil and Environmental Engineering, University of California, Los Angeles, Los Angeles, CA
[6] Department of Chemical and Biomolecular Engineering, University of California, Los Angeles, Los Angeles, CA
[7] California Nanosystems Institute, University of California, Los Angeles, Los Angeles, CA
[8] Department of Materials Science and Engineering, University of California, Los Angeles, Los Angeles, CA

** Corresponding authors: erika.laplante@uta.edu; gsant@ucla.edu*

ABSTRACT: We present the mass balances associated with carbon dioxide (CO_2) removal (CDR) using seawater as both the source of reactants, and as the reaction medium via electrolysis following the "*Equatic™*" (*formerly known as "SeaChange*") process. The process involves the application of an overpotential that splits water to form H^+ and OH^- ions, producing acidity and alkalinity, i.e., in addition to gaseous co-products, at the anode and cathode, respectively. The alkalinity that results, i.e., via the "continuous electrolytic pH pump" results in the instantaneous precipitation of calcium carbonate ($CaCO_3$), magnesium carbonates (Mg–CO_3), and/or magnesium hydroxide ($Mg(OH)_2$) depending on the CO_3^{2-} activity in solution. This results in the trapping, and hence durable and permanent (at least ~10,000–100,000 years) immobilization of CO_2 that was originally dissolved in water, and that is additionally drawn down from the atmosphere within: a) mineral carbonates, and/or b) as solvated bicarbonate (HCO_3^-) and carbonate (CO_3^{2-}) ions (i.e., due to the absorption of atmospheric CO_2 into seawater having enhanced alkalinity). Taken together, these actions result in the net removal of up to ≈4.6 kg of CO_2 per m^3 of seawater processed. Geochemical simulations quantify the extents of net CO_2 removal including the dependencies on the process configuration. It is furthermore indicated that the efficiency of realkalinization of the acidic anolyte using alkaline solids depends on their H^+ neutralization capacity and dissolution reactivity. We also assess changes in seawater chemistry resulting from $Mg(OH)_2$ dissolution with emphasis on the change in its alkalinity and saturation state. Overall, this analysis provides direct quantifications of the ability of the *Equatic™* process to serve as a means for technological CDR to mitigate the worst effects of accelerating climate change.

Keywords: Carbon dioxide mineralization, calcium carbonate, magnesium carbonate, brucite, carbon dioxide removal (CDR), electrolysis

INTRODUCTION AND BACKGROUND

The trapping of carbon dioxide (CO_2) as an aqueous (bi)carbonate ion (e.g., HCO_3^-, CO_3^{2-}) or as a mineral solid ("mineralization") is attractive because of favorable thermodynamics, and the safety and permanence of storage.[1–3] Furthermore, mineralization is a cost-effective pathway for CO_2 sequestration/removal (CDR), which at steady state, is estimated to cost <$100 per tonne (t) of CO_2.[1] During CO_2 mineralization, the release of Ca and Mg from the precursor solids is rate limiting, unless mass transport is limiting; which is seldom the case.[4] Thus, providing pre-solubilized cations that can readily react with CO_2 enormously facilitates mineralization rates and extents. Seawater is a vast reservoir of divalent cations (Ca, Mg) and dissolved CO_2 that can form sparingly soluble carbonates (and/or hydroxides). Long-term (millions of years) storage of CO_2 on Earth occurs by mineralization through the formation of calcite ($CaCO_3$) and aragonite ($CaCO_3$). But, over the short term, the abiotic precipitation of Ca- and Mg-carbonates from seawater is kinetically inhibited, as implied by the supersaturation of oceans with respect to these minerals.

The oceans absorb and immobilize atmospherically derived CO_2 in the form of dissolved carbonate species (i.e., predominantly HCO_3^- at a prevailing pH of ~8.1). Such aqueous immobilization is highly durable, although less so than mineral carbonate formation (i.e., with a stability of up to billions of years),[5,6] and presents a lower bound of stability in excess of 10,000 years.[7,8] As a result, 25% of all anthropogenic CO_2 emissions (~9 gigatonnes, Gt) are removed from the atmosphere by the oceans annually.[9] But, as a function of their prevailing chemistry, and ongoing ocean acidification, the capacity of the oceans to absorb any additional CO_2 (i.e., annually and per unit of seawater) is capped, unless prevalent CO_2 were to be removed. Toward this end, i.e., to remove CO_2 from the oceans and to expand the capacity of seawater to absorb additional CO_2, several electrochemical processes have been proposed, which focus on increasing ocean alkalinity via the: (a) production of OH^- from seawater (and the utilization of the HCl co-product to accelerate silicate weathering),[10] (b) using hard water and ion-exchange membranes,[11,12] or (c) utilizing pH swing processes to extract and capture CO_2.[13,14]

Recently, we proposed an approach to rapidly precipitate Ca- and Mg- carbonates and hydroxides from seawater to achieve CDR.[15] This *Equatic™* process electrolytically forces mineral carbonate precipitation thereby consuming prevalent CO_2 that is dissolved in seawater by locking it within carbonate minerals, and simultaneously producing alkaline mineral hydroxides that when dissolved in seawater enable the drawdown of atmospheric CO_2 into the seawater, representing net CO_2 removal.[15] This paper describes the CO_2 (mass) balances of this approach. Two scenarios are presented: (1) the precipitation of magnesium and calcium carbonates, i.e., a condition relevant to elevated carbonate activity, i.e., at super-ambient CO_2 concentrations, and (2) the precipitation of calcium carbonate and magnesium hydroxide ($Mg(OH)_2$: brucite), i.e., as relevant to ambient carbonate activity in seawater and atmospheric concentrations of CO_2. The analysis offers a quantitative basis for assessing the CDR potential of the technological approach and developing a robust measurement, reporting, and verification (MRV) strategy.

ANALYSIS METHODS

We use PHREEQC[16] to carry out detailed geochemical simulations. The llnl.dat database was used, which is appropriate for ionic strengths up to seawater salinity. The seawater composition used is based on Millero et al. (2008) (**Table 1**),[17] adjusted to pCO_2 (in atm) = -3.38 (420 ppm)[18] by charge balancing for the presence of inorganic C (carbon) species. The Saturation Index (SI) is defined as log Ω, where the saturation ratio, $\Omega = Q/K_{sp}$, and Q is the ion activity product and K_{sp} is the solubility product with respect to a given mineral. The saturation indices and ratios with respect to relevant Mg- and Ca-based minerals in seawater are shown in **Table 2**. In brief, seawater is supersaturated with respect to aragonite, calcite, dolomite, and magnesite, and undersaturated with respect to hydrated magnesium carbonates and brucite. All the calculations assume thermodynamic equilibrium for T = 25 °C, p = 1 bar (1 atm).

Table 1. The composition of seawater used in the analysis.

Species	Molality (*m*, mol/kg) based on Reference Composition[17]	Molality (*m*, mol/kg) after equilibration at 420 ppm $CO_{2(g)}$
Na^+	0.4860597	0.4860597
Mg^{2+}	0.0547421	0.0547421
Ca^{2+}	0.0106568	0.0106568
K^+	0.0105797	0.0105797
Sr^{2+}	0.0000940	0.0000940
Cl^-	0.5657647	0.5657647
SO_4^{2-}	0.0292643	0.0292643
HCO_3^-	0.0017803	0.0021002
Br^-	0.0008728	0.0008728
CO_3^{2-}	0.0002477	0.0000312
F^-	0.0000708	0.0000708
B [$B(OH)_4^-$, $B(OH)_3$]	0.0004303	0.0004303
H_2CO_3*	0.0000100	0.0000124
ΣCO_2	2.038 mmol/kg	2.141 mmol/kg
pH	8.352	8.170
pCO_2 (in atm)	–3.78	–3.38

Table 2. The saturation indices and ratios of different mineral solids in seawater.

Phase	Composition	Saturation Index, SI	Saturation Ratio, Ω
Aragonite	$CaCO_3$	0.52	3.311
Artinite	$Mg_2CO_3(OH)_2{\cdot}6H_2O$	–1.97	0.011
Brucite	$Mg(OH)_2$	–1.84	0.014
Calcite	$CaCO_3$	0.67	4.677
Dolomite	$CaMg(CO_3)_2$	3.26	1819.7
Huntite	$CaMg_3(CO_3)_4$	1.99	97.72
Hydromagnesite	$Mg_5(CO_3)_4(OH)_2{\cdot}4H_2O$	–3.38	0.0004
Lansfordite	$MgCO_3{\cdot}5H_2O$	–1.64	0.023
Magnesite	$MgCO_3$	0.97	9.333
Nesquehonite	$MgCO_3{\cdot}3H_2O$	–2.07	0.009

The CO_2 content (i.e., storage capacity) of seawater is dependent on its alkalinity. The total alkalinity (A_T, mg/L) of seawater is given by:

$A_T = [HCO_3^-] + 2\,[CO_3^{2-}] + [OH^-] + [B(OH)_4^-] + HPO_4^{2-}] + 2\,[PO_4^{3-}] + [H_3SiO_4^-] + [NH_3] + [HS^-] + 2\,[S^{2-}] - [H^+] - [HF] - [HSO_4^-] - H_3PO_4]$

or equivalently:

$A_T = [Na^+] + 2\,[Mg^{2+}] + 2\,[Ca^{2+}] + [K^+] + 2\,[Sr^{2+}] - [Cl^-] - [Br^-] + (\ldots) + \Sigma NH_3 + \Sigma NO_3 + \Sigma NO_2 + \Sigma PO_4 + \Sigma SO_4 + \Sigma F$

where (…) represents minor conservative species, $\Sigma NH_3 = NH_3 + NH_4^+$, $\Sigma NO_3 = NO_3^- + HNO_3$, $\Sigma NO_2 = NO_2^- + HNO_2$, $\Sigma PO_4 = H_3PO_4 + H_2PO_4^- + HPO_4^{2-} + PO_4^{3-}$, $\Sigma SO_4 = H_2SO_4 + HSO_4^- + SO_4^{2-}$ and $\Sigma F = HF + F^-$.[19–21]

RESULTS AND DISCUSSION

***Carbon dioxide dissolution in seawater*:** The equilibrium of gas-phase CO_2 with seawater is described in detail elsewhere.[22–24] Briefly, the dissolved CO_2 content in seawater is controlled by its pH, the atmospheric partial pressure of CO_2 (pCO_2), and the temperature as described by Henry's law. The relative concentrations of HCO_3^-, CO_3^{2-}, and H_2CO_3* which denotes the sum of H_2CO_3 (carbonic acid) and aqueous CO_2, $[HCO_3^-]$, $[CO_3^{2-}]$, and $[H_2CO_3^*]$, are determined via the equilibrium constants, K_H, K_1, and K_2 (see **Eq. 1-3**) which are functions of the temperature and the salinity of the water:[23]

$$[H_2CO_3^*] = K_H P_{CO_2} \quad \textbf{(Eq. 1)}$$

$$[HCO_3^-] = \frac{K_1}{[H^+]} \times [H_2CO_3^*] \quad \textbf{(Eq. 2)}$$

$$[CO_3^{2-}] = \frac{K_2}{[H^+]} \times [HCO_3^-] \quad \textbf{(Eq. 3)}$$

Here, **Eq. 1** is Henry's law, where K_H is the Henry's law constant (0.03428 mol/L/atm for freshwater (0 per mil, ‰) and 0.02858 for seawater (35 ‰)), and P is the partial pressure in atm (i.e., 420 ppm is equivalent to 0.00042 atm). The equilibrium constant, K_1 is taken as 4.498 × 10^{-7} mol/kg for freshwater and 14.52 × 10^{-7} mol/kg for seawater, whereas K_2 is taken as 0.479 × 10^{-10} mol/kg for freshwater and 11.12 × 10^{-10} mol/kg for seawater.[23,25] The concentration of aqueous H^+, is equivalent to 10^{-pH} (where the ionic product of water $K_w = 10^{-14}$). The speciation of CO_2 and the relative abundances of HCO_3^- and CO_3^{2-} show a strong dependence on the pH (**Fig. 1a**). On the other hand, H_2CO_3* is controlled by pCO_2 and is independent of pH. The equilibrium between H_2CO_3 and $CO_{2(aq)}$ is given by: $[H_2CO_3] = K_0[CO_{2(aq)}]$, where $pK_0 = 2.97$, indicating that $CO_{2(aq)}$ is ~1000 times more abundant than H_2CO_3.[26] Thus, the total dissolved CO_2 (total dissolved inorganic carbon: DIC, ΣCO_2) is given by the sum of the different carbon species and is equal to: $\Sigma CO_2 = [H_2CO_3^*] + [HCO_3^-] + [CO_3^{2-}]$. At pH 8.1 and 420 ppm CO_2, the total dissolved CO_2 concentrations in freshwater and seawater based on this analysis are 0.847 mmol CO_2/kg water and 2.557 mmol CO_2/kg water, in reasonable agreement with **Table 1** albeit with a discrepancy that is caused by differences in the equilibrium constants that are used.[27] Notably, the equilibrium ΣCO_2 in seawater is greater than that in freshwater because of the higher ionic strength of seawater that results in the speciation of CO_2 into HCO_3^- and CO_3^{2-} by complexation of the bicarbonate and carbonate ions with cations such as Na^+, Mg^{2+}, and Ca^{2+} (see **Fig. 1b**-**c**).

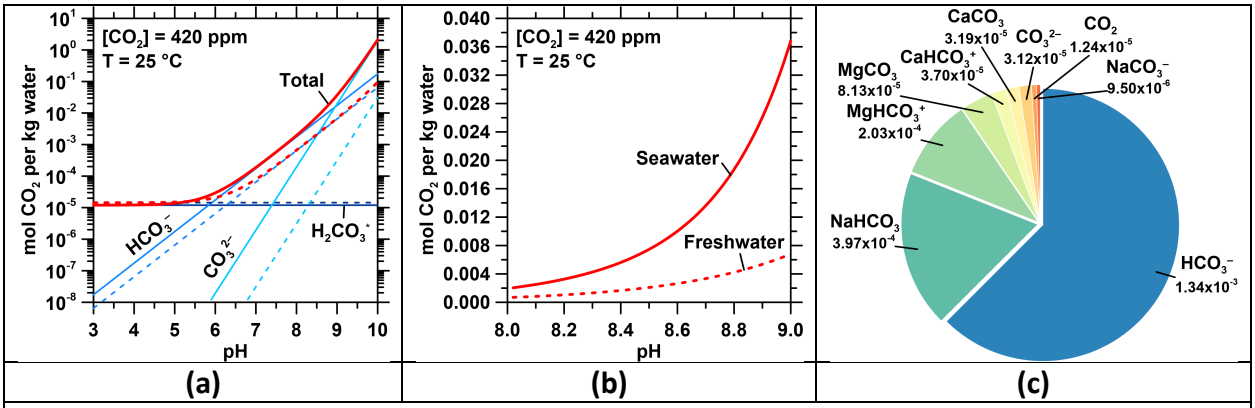

Figure 1. **(a)** The concentration and speciation of CO_2 in seawater (solid curves) and freshwater (dashed curves) in equilibrium with an ambient atmosphere containing 420 ppm CO_2 (0.042 vol. % CO_2). The total dissolved CO_2 is the sum of the concentrations of HCO_3^-, CO_3^{2-} and H_2CO_3*. H_2CO_3* represents the sum of $CO_{2(aq)}$ and true carbonic acid (H_2CO_3). The speciation of CO_2 is calculated using equilibrium constants that vary with temperature and salinity.[23] **(b)** The detail of **(a)** for 8≤pH≤9, showing the far greater solubility of CO_2 in seawater than freshwater. **(c)** The different aqueous species of dissolved inorganic carbon (DIC), including complexes with dissolved cations in seawater, and their relative amounts. The concentrations for each species are given in mol/kg (molal basis).

Electrolytic carbon removal: The *Equatic*^{TM} process consists of the following steps:
Step 1) The precipitation of magnesium carbonate (magnesite, $MgCO_3$, at super-ambient pCO_2; >1 atm)[28] or magnesium hydroxide and magnesium hydroxy-carbonates (at ambient pCO_2),
Step 2) The precipitation of calcium carbonate ($CaCO_3$),
Step 3a) The realkalinization of the anolyte stream to replenish the divalent cations, and
Step 3b) The dissolution of precipitated $Mg(OH)_2$ and the absorption of atmospheric CO_2 (**Fig. 2**) into a solution having an elevated pH. All the process steps including (3a-3b) occur prior to the discharge of the seawater effluent.[15]

Ultimately, the process traps CO_2 in: (a) dissolved (i.e., aqueous HCO_3^- and CO_3^{2-} species stabilized via the re-dissolution of $Mg(OH)_2$) and/or, (b) solid (e.g., $CaCO_3$, a mineral carbonate) forms. This manner of CDR is represented by two limiting cases: (**Case 1**) $CaCO_3$ + $Mg(OH)_2$ (i.e., 89 mass % aqueous, 11 mass % solid CO_2 immobilization), and (**Case 2**) $CaCO_3$ + $MgCO_3$ (i.e., 100 mass % solid CO_2 immobilization), and **(Case 3)** which implies the formation of a mixture of $Mg(OH)_2$ and $MgCO_3$ alongside $CaCO_3$. The solids produced via this process, predominantly $CaCO_3$, can be discharged back into the ocean, where they will remain stable because of their native prevalence and persistence (e.g., seashells in the ocean), and seawater's supersaturation with respect to these mineral carbonates (**Table 2**), or beneficially utilized, e.g., as sand in concrete, or as a carbon-neutral source to produce cement. Obviously, if hydrated carbonate phases including nesquehonite ($MgCO_3{\cdot}3H_2O$), lansfordite ($MgCO_3{\cdot}5H_2O$), hydromagnesite ($Mg_5(CO_3)_4(OH)_2{\cdot}4H_2O$), and dypingite ($Mg_5(CO_3)_4(OH)_2{\cdot}5H_2O$) form, alternative disposal strategies (e.g., on land) will need to be used due to the tendency of these solids to dissolve if they were discharged into seawater (**Table 2**).

From stoichiometry, the formation of 1 mole of $CaCO_3$ or $MgCO_3$ captures 1 mole of CO_2, while requiring 2 moles of OH^-. For comparison, only 1.2 moles of OH^- are required per mole of CO_2 stored as dissolved (bicarbonate: HCO_3^- and carbonate: CO_3^{2-}) ions (**Fig. 1** and **7**).[7,15] This implies that per unit of alkalinity, it is more chemically and energy efficient to store CO_2 in the form of dissolved aqueous carbonates, i.e., rather than mineral carbonate species. The *Equatic*^{TM} process is based on the electrolysis of seawater. Such electrochemical stimulation of seawater implies the formation of alkalinity (OH^-) at the cathode, and acidity (H^+) at the anode. In addition, gas phase co-products evolve, including hydrogen ($H_{2(g)}$) at the cathode, and oxygen ($O_{2(g)}$) and chlorine ($Cl_{2(g)}$) at the anode. These gas evolutions are described by the hydrogen evolution reaction (HER), oxygen evolution reaction (OER), and chlorine evolution reaction (ClER), respectively. During seawater electrolysis, unless an oxygen-selective anode is used, ClER is the predominant reaction at the anode because its $2e^-$ basis (i.e., as compared to the $4e^-$ basis of OER) makes it kinetically more favorable.

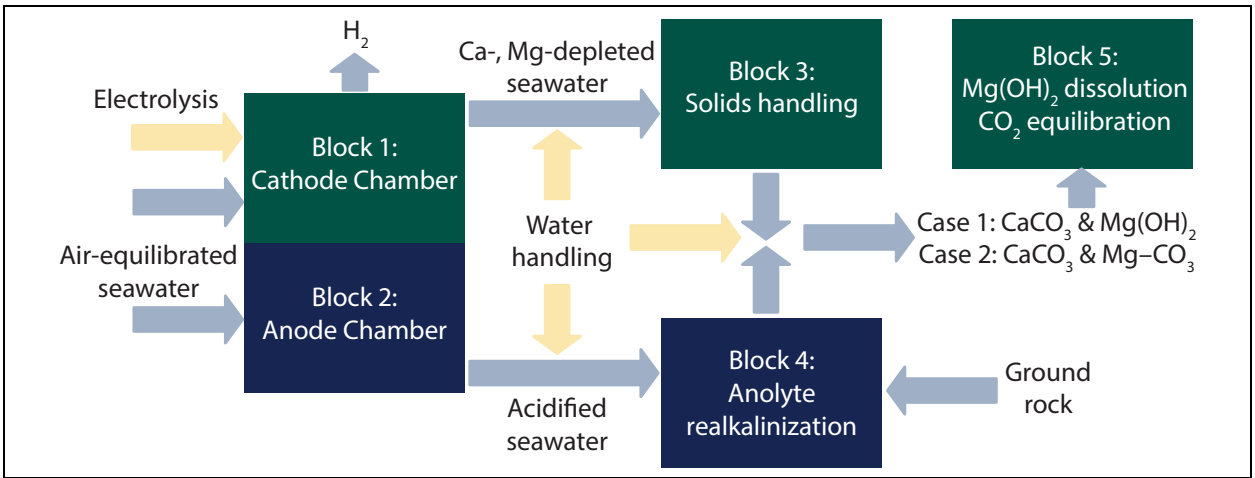

Figure 2. A schematic of the *Equatic*^{TM} process showing the inlet and outlet feeds and energy requirements of the primary steps for CO_2 removal as: carbonate solids and (aqueous) dissolved CO_2 (**Case 1**) and carbonate solids only (**Case 2**). The major energy inputs include electrolysis, water handling, and rock grinding.[15]

The *Equatic*^{TM} process can be examined for a system that removes 1 t of CO_2 per day (TPD). This system requires the processing of ~220 m^3 per day of seawater to yield 235 kg of $CaCO_3$ and 702 kg of $Mg(OH)_2$ (i.e., if the solids were suspended in the solution this translates to ≈3.3 mass % solids, corresponding to a dilute system) while assuming a CO_2 removal efficiency of 1.7 mol CO_2 per mol $Mg(OH)_2$ (see below). In addition, ~29 kg of $H_{2(g)}$, ~46 kg of $O_{2(g)}$, and ~818 kg of chlorine ($Cl_{2(g)}$, HClO, and ClO^-) are produced when using an anode that is not OER-selective (e.g., platinum). The amount of free chlorine generated can be reduced greatly by the use of oxygen-selective anodes, without compromising the overpotential, and achieving >98 mass % selectivity to the OER as compared to ClER – a fast maturing effort which addresses obvious issues related to toxicity, handling, and atmospheric release of chlorine, and chlorine derivatives. For these considerations, **Case 1** yields net 4.6 kg of CO_2 removal per m^3 of seawater. For **Case 1**, CO_2 removal via the alkalinity enhancement enabled by the dissolution of

brucite ($Mg(OH)_2$) can be effected in the ocean, i.e., following discharge of the brucite, or within a captive carbonation/aeration reactor wherein air is pumped/bubbled into the solution and CO_2 absorption and bicarbonate/carbonate ion formation occur following Henry's Law (further discussion below) (**Fig. 2**).

Alternatively, **Case 2** requires 348 m^3 per day of seawater and will produce 371 kg of $CaCO_3$ and 1606 kg of $MgCO_3$ (i.e., if the solids were suspended in the solution this translates to ≈5.7 mass % solids, corresponding to a dilute system). In addition, ~46 kg of $H_{2(g)}$, ~73 kg of $O_{2(g)}$, and ~1295 kg of free chlorine ($Cl_{2(g)}$, HClO, and ClO^-) are produced when using a platinum-based anode that is not OER-selective. Thus, **Case 2** yields net 2.9 kg of CO_2 removal per m^3 of seawater. It should be noted, however, that **Case 2** requires elevated pCO_2 to force the precipitation of $MgCO_3$, even at high pH. As such, **Case 2** implies the bubbling of concentrated CO_2 into seawater, and therefore requires integration with a fractional direct air capture (DAC) system or a CO_2-enriched flue gas emissions stream. The mass and energy inputs relevant to **Case 1** and **Case 2** are shown schematically in **Figure 2** and are described elsewhere.[15]

Precipitation of calcium carbonate and magnesium hydroxide: The ocean is supersaturated with respect to aragonite by factors of at least 2-3 (**Table 1**), implying that the kinetic inhibition of precipitation is operative.[29] With decreasing Ω, the time elapsed before the onset of precipitation increases gradually at Ω > 3 and then sharply at Ω ~3, implying seawater stability at Ω < 3.[30] This kinetic inhibition of precipitation is caused by dissolved organic matter,[31,32] phosphate ions,[33] magnesium ions,[34] and sulfate ions.[35] To overcome the kinetic hindrance to precipitation we alkalinize the electrolyte such that, e.g., at pH 10-12, in the vicinity of the cathode we ensure Ω > 1400 (at pH 10) for calcite, and Ω > 7 (at pH 10) for brucite for a solution in equilibrium with air: i.e., saturation ratios which are more than sufficient to overcome the thermodynamic and kinetic barriers to mineral precipitation.

If uncompensated, the precipitation of Ca and Mg-minerals from seawater at the cathode would lead to a net lower seawater pH and hence a reduction in its dissolved CO_2 storage capacity; as a function of CO_2's pH-dependent solubility in water (**Fig. 3a**). Similarly, the decrease of the pH of the anolyte in an electrolysis system to pH≈1 results in CO_2's degassing to a limit of 2.141 mmol CO_2/kg seawater as described by Henry's law (**Fig. 1a**). But on the other hand, the net increase in the pH of the catholyte, on account of the electrolytic pH pump, and the subsequent dissolution of brucite, increases the amount of CO_2 absorbed very significantly (**Fig. 1a**), far exceeding the amount of CO_2 degassed at the anolyte. For example, maintaining a fixed catholyte pH of 8.5, 9.0, and 9.5, just within the electrolytic reactor and not including the OH^- liberated following the dissolution of brucite, yields an *additional* 2.787, 17.72, and 86.54 mmol CO_2/kg water of storage vis-à-vis the native pH of seawater (≈8.1) [N.B.: under operational conditions, the electrochemical reactors maintain a pH≈10-12 in the vicinity of the cathode]. This suggests that the *Equatic™* process can be used to enhance seawater's CO_2 storage capacity, while also accomplishing atmospheric CO_2 removal. This is in contrast to traditional direct air capture (DAC) processes since a decrease in atmospheric CO_2 concentrations, if effected in isolation via DAC, would result in the degassing of CO_2 from the oceans on account of the ocean-atmosphere partitioning equilibrium of CO_2 (**Eq. 1**).[15,36]

Expectedly, if the catholyte effluent is not in equilibrium with atmospheric CO_2, re-equilibration, i.e., the progressive absorption of CO_2 from the air will decrease its pH (**Fig. 3b**). Thus, our simulations show that an exit (effluent) pH≈11.5 is required to maintain a pH ≥ 8.5 upon equilibration with atmospheric CO_2, for a catholyte effluent that is depleted in aqueous Ca^{2+} and Mg^{2+} ions (i.e., where Ca and Mg are contained within mineral solids). It is furthermore important to highlight that in the *Equatic*^{TM} process, due to the provisioning of a continuous (electrolytic) pH pump, the precipitation of mineral carbonates does not result in the degassing of CO_2 (i.e., due to acidification that results from the deprotonation of bicarbonate ions: HCO_3^-, during carbonate mineralization), as is the case for non-electrolytically stimulated conditions.

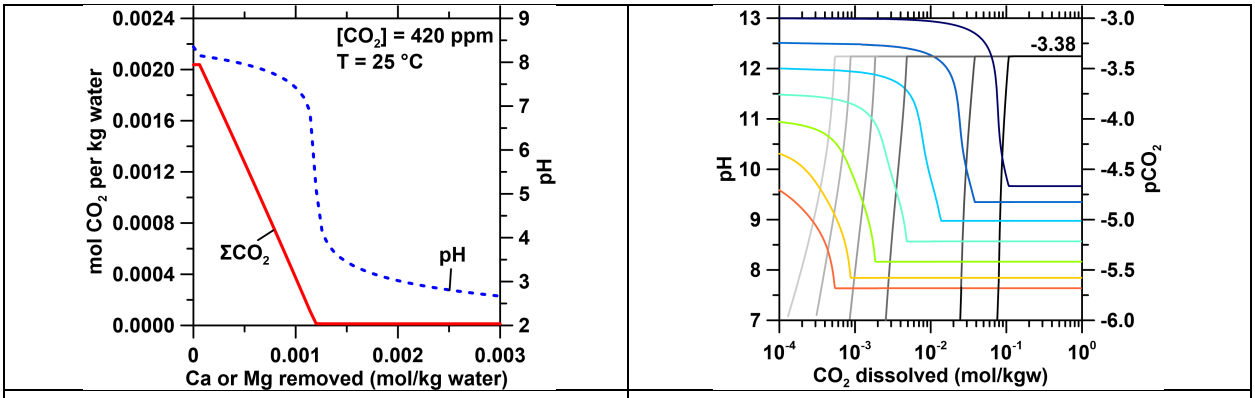

(a) **(b)**

Figure 3. **(a)** The evolution of total dissolved CO_2 (ΣCO_2) and the pH of seawater with increasing Ca^{2+} and Mg^{2+} precipitation as $CaCO_3$, $MgCO_3$ and/or $Mg(OH)_2$, **(b)** The equilibration with air of the catholyte effluent for pHs ranging from 9.5 to 13, where the catholyte is depleted of divalent cations and CO_2. The figure shows different extents of pH decrease (red–blue curves) with progressive CO_2 absorption as pCO_2 (gray curves) approaches –3.38 (i.e., atmospheric concentrations). For pCO_2 evolution, increasing darkness of the gray curves corresponds to increasing initial pH of the catholyte effluent.

Realkalinization of the catholyte and anolyte effluent: The discharge of the catholyte (i.e., depleted of Ca and Mg) and anolyte (i.e., an acidic solution) effluent into the ocean could result in changes in seawater chemistry and saturation states (e.g., a decrease in SI with respect to aragonite, a reduced CO_2 storage capacity, etc., **Table 2**, **Table 3**). To counter such effects requires the remineralization of the effluent by the dissolution of alkaline minerals such as those found in mafic and ultramafic rocks into the anolyte, to elevate the concentrations of divalent cations. Candidate solutes for this include pyroxenes (e.g., augite $[(Ca,Na)(Mg,Fe,Al,Ti)(Si,Al)_2O_6]$, diopside $[MgCaSi_2O_6]$) and olivines (e.g., forsterite $[Mg_2SiO_4]$) that naturally occur in mafic (basalts, gabbro) and ultramafic (peridotites) rocks. As Ca^{2+} and Mg^{2+} species are dissolved into the effluent, its pH and total dissolved CO_2 content elevate (**Fig. 4**). It is evident that an increase in the ΣCO_2 occurs only when the pH exceeds ~5 (**Fig. 1a**). Furthermore, the replenishment of the cations increases not only the pH but also the salinity, enabling further CO_2 absorption (**Fig. 1b-c**, **4b**) – a reason why seawater contains much more dissolved CO_2 than freshwater.

Table 3. The representative steady-state composition of the anolyte and catholyte effluent exiting the electrolyzer (see **Fig. 2**).

Species	Anolyte Molality (mol/kg) after equilibration at 420 ppm	Catholyte Molality (mol/kg)
Na^+	0.4110597	0.6228000
Mg^{2+}	0.0547421	0
Ca^{2+}	0.0106568	0.0083568
K^+	0.0105797	0.0105797
Sr^{2+}	0.0000940	0.0000940
Cl^-	0.6367647	0.5680000
SO_4^{2-}	0.0292643	0.0292643
HCO_3^-	1.106×10^{-10}	0
Br^-	0.0008728	0.0008728
CO_3^{2-}	1.506×10^{-19}	0
F^-	0.0000708	0.0000708
B [$B(OH)_4^-$, $B(OH)_3$]	0.0004303	0.0004303
H_2CO_3*	0.0000164	0
ΣCO_2	0.0000164	0
$CaCO_3$ (s)	0	0.002
$Mg(OH)_2$ (s)	0	0.055
pH	1.023	12.200
pCO_2	–3.38	-

The quantity of rock required to replenish the cation abundance, and the pH of the combined (catholyte and anolyte) effluent is a function of the solute's acid ($[H^+]$, proton) neutralization capacity (ANC). This capacity can be calculated from the solute's oxide composition assuming progressive dissolution, and a dissolution reaction (congruent: stoichiometric (e.g., $Mg_2SiO_{4(s)}$ (forsterite) + $4H^+ \rightarrow 2Mg^{2+} + H_4SiO_4$), or incongruent: non-stoichiometric (e.g., $CaAl_2Si_2O_{8(s)}$ (anorthite) + $2H^+ + H_2O \rightarrow Ca^{2+} + Al_2Si_2O_5(OH)_{4(s)}$)).[4] For simplicity we consider complete and congruent dissolution (**Table 4**, **Fig. 5**) to identify the maximum ANC. A range of compositions for these minerals yield ANCs of up to ≈50 mol H^+/kg solid (i.e., for MgO). This translates to a theoretical mass (and volume) requirement of 1.60 g Mg_2SiO_4/g CO_2 sequestered (0.49 cm^3 Mg_2SiO_4/g CO_2) or 2.36 g $CaAl_2Si_2O_8$/g CO_2 (0.86 cm^3 $CaAl_2Si_2O_8$/g CO_2) to replenish Mg^{2+} or Ca^{2+} removed by $MgCO_3$ and $CaCO_3$ precipitation (**Case 2**). For **Case 1**, since the dissolution of $Mg(OH)_2$ will autogenously replenish Mg^{2+} in seawater, only Ca^{2+} depletion needs to be considered, resulting in a solid requirement of 0.76 g $CaAl_2Si_2O_8$/g CO_2 (0.28 cm^3 $CaAl_2Si_2O_8$/g CO_2). However, to additionally neutralize the acidity of the anolyte (i.e., OH^- from $Mg(OH)_2$ dissolution is counted toward CO_2 sequestration and thus cannot be double counted for acidity neutralization), an additional quantity of 1.07 g Mg_2SiO_4/g CO_2 (0.45 cm^3 Mg_2SiO_4/g CO_2) is required.

The lower alkalinity requirement for **Case 1** is a result of the greater CO_2 removal efficiency of $Mg(OH)_2$ compared with $MgCO_3$ (i.e., since only 1.2 moles of OH^- are required per mole of CO_2 stored as dissolved bicarbonate (HCO_3^-) ions). For either case, if the catholyte effluent, i.e., including the suspended solids were to be discharged into the ocean, the $CaCO_3$ and $MgCO_3$ (if any) that are present would remain stable, i.e., they would not dissolve given the significant oversaturation of the oceans with respect to these minerals (see **Table 2**). That said, we recognize that effluent alkalization (i.e., ensuring equivalence of the pH of the influent and the combined, anolyte + catholyte effluent), and divalent cation regeneration (i.e., abundances of Ca and Mg in the influent and combined effluent are equal) are prerequisite to discharge the effluent back into the ocean. But, beyond chemical considerations, other aspects require further work. For example, it is known that the [Ca/Mg] ratio in the oceans is of relevance to calcifying organisms, particularly the stability of their calcified exoskeletons in an acidifying ocean.[37–40] While we cannot yet assess if the *Equatic*^{TM} process, if globally deployed for 10s of gigatonnes of CDR annually would affect such aspects (albeit, not at the scale of single plants), further work is needed to better understand these details in due course.

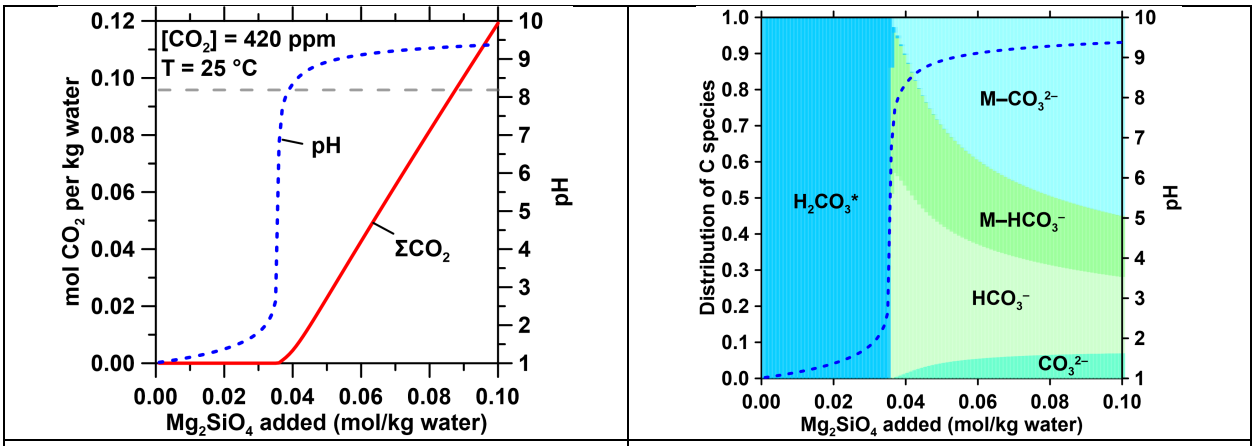

Figure 4. **(a)** The total dissolved inorganic carbon (ΣCO_2) in the anolyte following dissolution (alkalinization) of Ca- or Mg-rich solids (e.g., Ca_2SiO_4 or Mg_2SiO_4). A dashed gray line indicates typical ocean pH. **(b)** The distribution of inorganic carbon species as a function of the extent of realkalinization, showing the persistence of H_2CO_3* at low(er) pH, and HCO_3^- and CO_3^{2-} at high(er) pH. M–HCO_3^- and M–CO_3^{2-} represent aqueous HCO_3^- and CO_3^{2-} complexes with Na^+, Ca^{2+}, and Mg^{2+}.

Olivine $(Mg,Fe^{2+})_2SiO_4$ is the most abundant mineral (ultramafic, and otherwise) in the Earth's upper mantle. On the Earth's surface, olivine is primarily found in ophiolites, which are sections of the uppermost mantle and oceanic crust that are exposed on land by tectonic activity, and that are found worldwide along convergent and divergent plate boundaries. Ophiolites are composed of a specific sequence of mafic (basalt, gabbro) and ultramafic (peridotites such as harzburgite, dunite) rocks and can have thicknesses on the order of 5 to 10 km and encompass areas exceeding ~100,000 km^2.[41,42] Peridotites are intrusive rocks that are

classified based on the amounts of olivine, clinopyroxene ($(Ca,Na,Li)(Mg,Fe^{2+},Al,Fe^{3+})Si_2O_6$), and orthopyroxene ($(Mg,Fe)Si_2O_6$). In ophiolites, lherzolite, harzburgite, and dunite peridotites are most common, containing at least 40 mass % olivine. Assuming a thickness of 1 km, and an area of 10,000 km^2, and 50 mass % fosteritic olivine (Mg_2SiO_4), leads to a volume of 5,000 km^3, substantially exceeding the volume of olivine needed to sequester all anthropogenic CO_2 emitted into the atmosphere, i.e., including ongoing (17 km^3 per year; ~36 Gt per year) and all legacy emissions (1225 km^3; ~2500 Gt since 1850).[43] In other words, if appropriately harvested, natural mafic and ultramafic rocks and minerals are an effectively limitless supply of alkalinity for CO_2 management. Beyond such rocks, industrial processes produce ~7 Gt of alkaline solids per year, including (but not restricted to) products and by-products such as lime (~430 Mt), cement kiln dust (~478 Mt), slags (~516 Mt), and coal ash (~701 Mt).[44,45]

Table 4. The diversity of alkaline solids that can be used for effluent alkalinization ordered as a function of their stoichiometric acid neutralization capacity (ANC).

Solute	Description	ANC (mol H^+/kg solid)
Periclase	MgO, a mineral found in metamorphic rocks	49.63
Lime	CaO, can be naturally occurring or synthetic	35.66
Lime kiln dust[46]	By-product of lime manufacturing	34.38
Forsterite	Mg_2SiO_4, the Mg-endmember of olivine	28.43
Olivine[47]	Group of nesosilicate minerals found in ultramafic rocks	25.97
Larnite	Ca_2SiO_4, a nesosilicate found in crystalline slags	23.22
Serpentinite	Ultramafic rock rich in serpentine, a hydrothermal alteration product of olivine	22.96
Basalt	Fine-grained mafic rock rich in plagioclase feldspar and pyroxene	22.91
Stainless steel slag	Semicrystalline by-product of metal manufacturing	22.02
Peridotite	Ultramafic rock rich in olivine with some pyroxene	22.00
Lizardite (Serpentine)	$Mg_3(Si_2O_5)(OH)_4$, a phyllosilicate	21.65
Ladle slag	Semicrystalline by-product of metal manufacturing	20.40
Blast furnace slag[48]	Semicrystalline by-product of metal manufacturing	19.97
Diopside	$CaMgSi_2O_6$, a single-chained inosilicate (pyroxene)	18.47
Air-cooled blast furnace slag	Crystalline by-product of metal manufacturing	17.78
Wollastonite	$CaSiO_3$, a single-chained inosilicate	17.22
Basic oxygen furnace slag	Semicrystalline by-product of metal manufacturing	16.85
Brownmillerite	$Ca_2(Al,Fe^{3+})_2O_5$, a non-stoichiometric perovskite	16.66
Comingled electric arc furnace slag	Semi-crystalline by-product of metal manufacturing	16.64

Cement kiln dust[48]	Amorphous by-product of Ordinary Portland Cement (OPC) production	15.94
Talc	$Mg_3Si_4O_{10}(OH)_2$, a phyllosilicate	15.82
Electric arc furnace slag	Semi-crystalline by-product of metal manufacturing	15.08
Class C fly ash	High-calcium fly ash from processing subbituminous and lignite coals	13.59
Reclaimed Class C fly ash	High-calcium fly ash reclaimed from landfill	13.45
Anorthite	$CaAl_2Si_2O_8$, Ca-endmember of plagioclase feldspar, a tectosilicate	9.61
Trona-rich fly ash	Fly ash containing $Na_3(CO_3)(HCO_3)\cdot 2H_2O$	9.44
Bytownite	$Na_{0.2}Ca_{0.8}Al_{1.8}Si_{2.2}O_8$, a type of plagioclase feldspar, a solid solution of $NaAlSi_3O_8$ and $CaAl_2Si_2O_8$	6.55
Gabbro	Coarse-grained mafic rock rich in plagioclase feldspar and pyroxene	6.48
Anorthosite	Fine-grained mafic rock rich in anorthite	5.65
Albite	$NaAlSi_3O_8$, Na-endmember of plagioclase feldspar, a tectosilicate	3.80
Class F fly ash	Low-calcium fly ash from processing anthracite and bituminous coals	1.91

The Goldich stability series indicates that the relative reactivity of silicate minerals is dependent on their crystallization temperatures, i.e., minerals formed at higher temperatures are more reactive than those formed at lower temperatures (**Fig. 6a**). This is further reflected in the degree of polymerization of tetrahedral silicate units, i.e., in general, a higher Si to O ratio signifies greater polymerization and lower temperature of cooling. For example, comparing the reactivities of anorthite and forsterite, both abundant silicates that are reservoirs of Ca and Mg, reveals that forsterite is more reactive owing to its structure in which all SiO_4^{4-} units are connected to each other by Mg^{2+} ions.[49,50] On the other hand, anorthite features a framework silicate structure with extensive sharing of O atoms by Si.[51] In addition, kinetic considerations such as the rates of water exchange around the cations also influence reactivity; for instance, Ca-based silicates dissolve faster than Mg-based silicates despite having an *equivalent* (crystallographic) structure due to the stronger solvation-state of Mg as compared to Ca.[52] Using data from Pokrovsky and Schott (2000),[49] the rate of forsterite dissolution as a function of pH for 1 < pH < 7 can be expressed as $R = 2.376 \times 10^{-11}\, e^{-1.15(pH)}$, where R is the dissolution rate in mol/cm^2/s (see **Fig. 6a**). Using this relation, the dissolution rates at pH 1, 2, 3, 4 can be estimated as 7.53×10^{-12}, 2.38×10^{-12}, 7.54×10^{-13}, and 2.39×10^{-13} mol/cm^2/s, respectively. For a non-porous sphere, i.e., where the external surface area is all that is reactive, the specific surface area (SSA) and particle diameter (d) are related by: $d = 6/(SSA \times \rho)$, where ρ is the density (**Fig. 6b**). The effect of specific surface area on the mass-normalized dissolution rate can be estimated to assess the fineness of particles and the residence time in a column reactor that are required to achieve the rate and extent of mineral dissolution in the highly acidic anolyte sufficient to ensure divalent cation abundance renewal, and therefore realkalization (**Fig. 6c**).

The rate equations can also be used to calculate time-dependent pH evolution during mineral dissolution. For example, progressively dissolving 50 kg of forsterite (d_{50} = 10 µm) in 1000 kg of water (initial pH = 1) results in the production of ~60 mol Mg^{2+} (60 mmol Mg^{2+}/kg) within 24 h. For comparison, ~80 mmol Mg^{2+}/kg is required to raise the pH of the anolyte from ~1 to ~8.2 (i.e., native seawater pH) (**Fig. 4a**). Decreasing the particle size increases the dissolution rate, at an energy expense. For instance, using a Bond Work Index approach, for silicate rocks, we estimate a grinding energy of around 70 kJ per kg rock is needed to produce particles with d_{50} ~ 100 µm for dissolution. Significantly, the intense acidity (pH~1) of the anolyte effluent that is generated herein is useful in that it enables accelerated silicate dissolution.

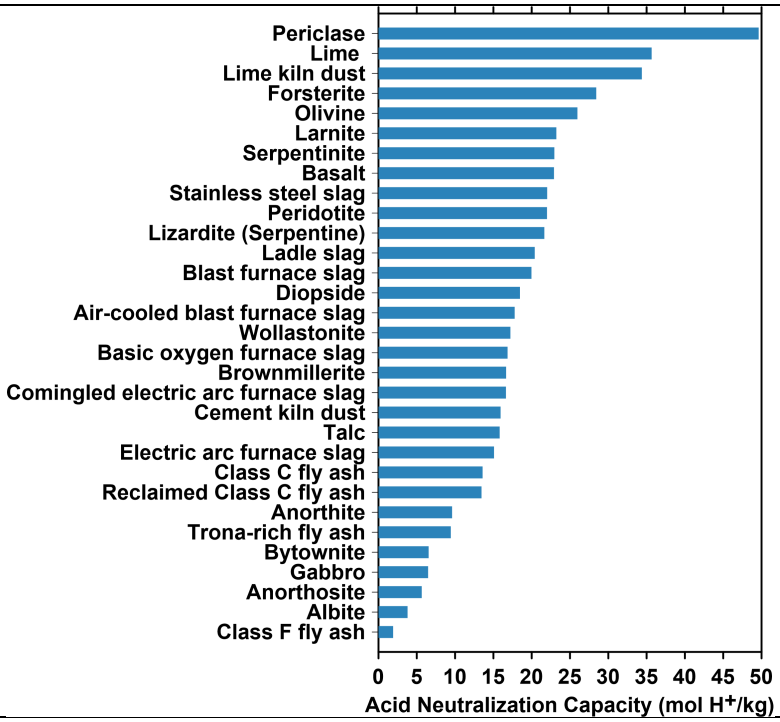

Figure 5. The acid neutralization capacity (ANC: i.e., the effluent realkalinization potential) of diverse alkaline solids (**Table 4**). While exact abundances are non-trivial to assess, these materials are available at levels ranging from 10s-to-100s of millions (e.g., slags) to 1000s of billions of tonnes (e.g., olivine).

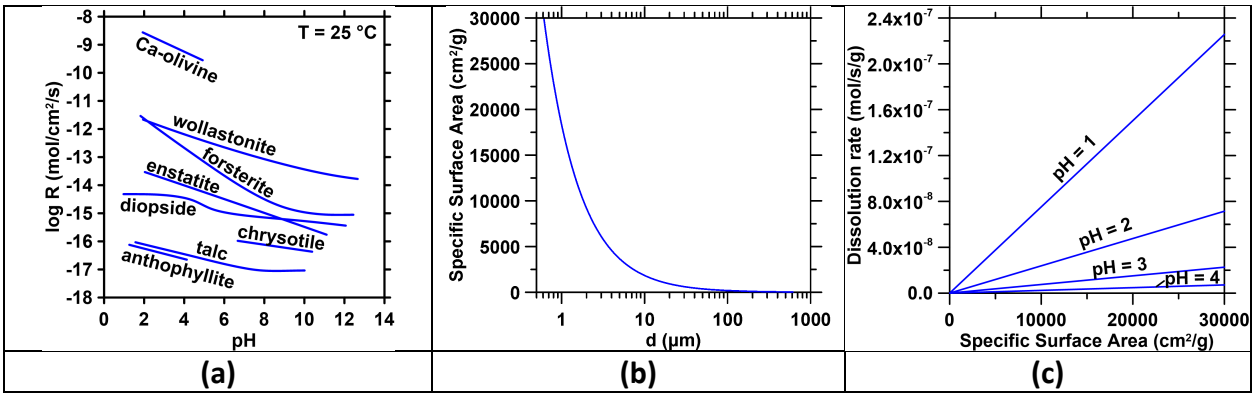

Figure 6. **(a)** The dissolution rate of Ca and Mg silicates at 25 °C as a function of pH, following Schott et al. (2009).[50] **(b)** The dependence of the specific surface area on the diameter, assuming mono-sized spherics, and **(c)** The mass-normalized dissolution rate of forsterite as a function of the specific surface area for select anolyte pHs, calculated from **(a)** and **(b)**.

Dissolution of brucite: A range of diverse processes including riverine input, atmospheric and evaporite cycling, ion exchange, hydrothermal activity, low-temperature basalt weathering, and carbonate deposition control the input–output balance of divalent seawater ions (Ca, Mg) and the net change in seawater's alkalinity.[53] Natural processes result in a net flux for Ca that is zero (i.e., the amount added to the oceans is equal to the amount removed from the oceans by carbonate deposition) and a net decrease in Mg concentration by 1.5×10^{12} mol per year.[53] **Case 1** implies the dissolution of brucite in seawater, in which seawater is undersaturated with respect to, raising its pH thereby drawing down atmospheric CO_2 thereby ensuring net CDR. The dissolution of brucite progressively increases seawater's pH expanding its CO_2 storage capacity (**Fig. 7a**) such that between 1.3-to-1.7 mol of CO_2 are absorbed per mol of $Mg(OH)_2$ (**Fig. 7b**).

Under static/batch conditions (i.e., R_e~0, where R_e is the Reynolds number, unitless) where there is very slow dissipation of dissolved species, locally, it is possible that increases in the alkalinity of seawater, e.g., caused due to brucite dissolution, could result in alterations of mineral saturation states. This could induce secondary carbonate formation (see **Fig. 8**) since the increase in alkalinity shifts the HCO_3^-–CO_3^{2-} distributions (e.g., see the Bjerrum diagram for dissolved inorganic speciation) in seawater thereby facilitating aragonite precipitation via the combination of Ca^{2+} and CO_3^{2-} species. Thus, in circumstances wherein brucite-containing effluent is discharged into the oceans it is necessary to examine how quickly: a) brucite may dissolve?, and b) how quickly dissolved brucite species (i.e., particularly alkalinity) may be dissipated? While the release of CO_2 that typically accompanies secondary carbonate precipitation is not an issue (i.e., where the release of CO_2 occurs via bicarbonate rather than carbonate combination with calcium species via the reaction: $Ca^{2+} + 2HCO_3^- \rightarrow CaCO_3 + CO_2 + H_2O$, such that 1 mol CO_2 is released per mol $CaCO_3$ precipitated)[54] in the presence of added alkalinity (i.e., $Mg(OH)_2$ dissolution), this aspect should nevertheless be considered in further detail because: a) $CaCO_3$ precipitation will consume OH^-, decreasing the efficiency of CO_2 absorption (**Fig. 7b, 7d**) since it is more efficient to stabilize atmospheric CO_2 as aqueous species than within mineral carbonates, and b) it could change locally, and at short time scales the [Ca/Mg] ratios in seawater.

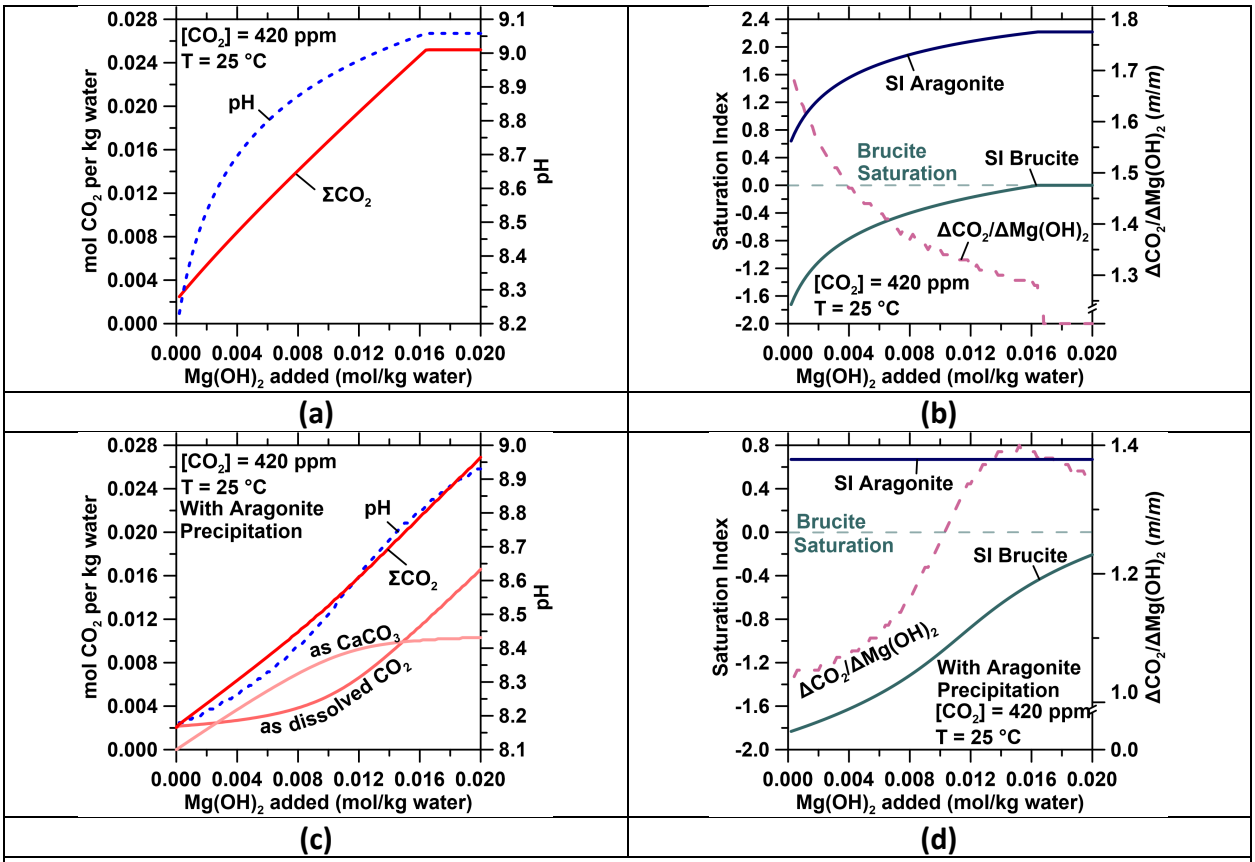

Figure 7. The effect of the extent of $Mg(OH)_2$ addition/dissolution on the **(a)** total dissolved carbon and pH, and **(b)** saturation indices of seawater with respect to aragonite and brucite. The molar effectiveness of $Mg(OH)_2$ addition for CO_2 removal for each 0.0002 *m* addition of $Mg(OH)_2$ is also shown. Similar plots for a case where aragonite precipitation occurs in excess of the original saturation index of seawater are shown in **(c)** and **(d)**.

At seawater pH, the dissolution rate of brucite is on the order of 10^{-8} mol/m^2/s.[55] To achieve CO_2 removal at the level of 10 Gt/year would require the dissolution of 8.3 Gt of $Mg(OH)_2$ corresponding to the addition of 1.1×10^{-7} mol $Mg(OH)_2$/kg seawater. If brucite dispersion is assumed to be averaged across the world's oceans, an unrealistic and impractical assumption, changes in seawater pH and mineral saturation indices are irrelevant. For context, the critical saturation ratio, Ω, for runaway aragonite precipitation is 5 (SI = 0.69).[56] Using a model that considers ocean circulation, i.e., ECCO (Estimating the Circulation and Climate of the Ocean) LLC270 physical fields,[57] and constraints of ΔpH = 0.1 and $\Delta\Omega_{aragonite}$ = 0.5, regions within 300 km of the coast can accommodate 100s of megatons of atmospheric CO_2 removal.[58] This shows that simple near-coastal alkalinity discharge, such as that proposed herein, can scale to several Gt per year if spread over available coastlines.[58]

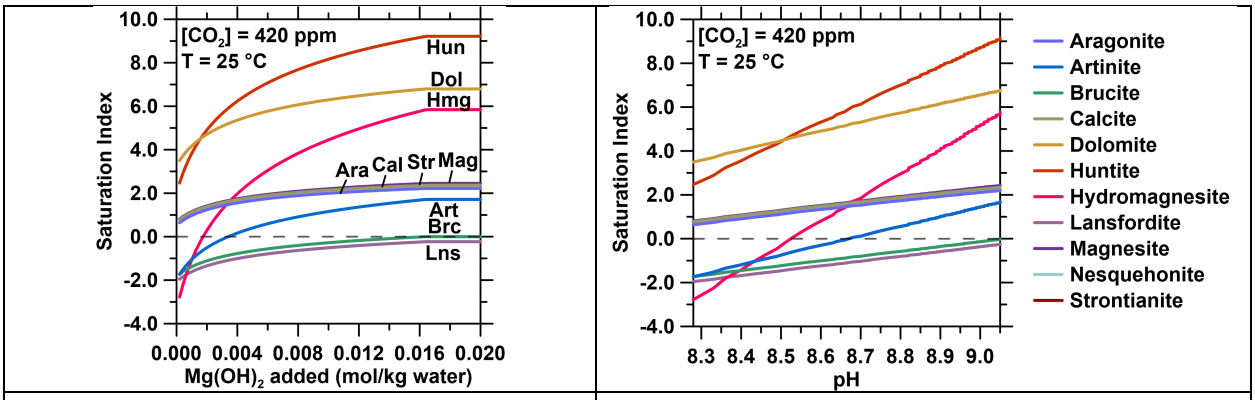

(a) **(b)**

Figure 8. The changes in the mineral saturation indices of diverse minerals with **(a)** increasing $Mg(OH)_2$ dissolution or **(b)** increasing pH, see also **Table 2**.

An important question related to the *Equatic*^{TM} process involves answering the question: *"What is the best approach for $Mg(OH)_2$ dissolution and atmospheric CO_2 drawdown: i.e., in the open ocean, or within an (industrial) plant?"* Each approach has distinct benefits and challenges. First, we can consider the case wherein brucite dissolution occurs following the discharge of the calcite and brucite (particulate) containing effluent into the ocean ("in ocean" approach). This requires two steps leading to CO_2 removal: **Step A)** brucite dissolution, and **Step B)** CO_2 drawdown from the atmosphere. At high brucite undersaturations and moderate convective conditions (for comparison, the turbulence in oceans varies by at least 8 orders of magnitude with characteristic R_e reports of 70 and 4×10^8),[59–61] the dissolution of brucite is rapid requiring on the order of a few to 10s of hours. On the other hand, the equilibration of air and sea (i.e., gas-liquid CO_2 concentrations) occurs over weeks to months depending on the mixed layer depth and wind speed.[62] Therefore, to achieve atmospheric CO_2 drawdown, $Mg(OH)_2$ must not only fully dissolve but also the alkalinized seawater must remain in the mixed layer during this period. This results in an uncertainty regarding the amount of time and the extent of CO_2 absorbed required for carbon dioxide drawdown from the atmosphere.

Second, we can consider a process configuration wherein air is bubbled into the brucite-containing catholyte within a high surface-to-volume (s/v, m^{-1}), high mass transfer rate aeration reactor, i.e., inside-the-battery limit ("ISBL" approach) of an industrial plant. While such aeration requires bubbling ~2500 t of atmospheric air to derive ~1 t of CO_2 (assuming ~420 ppm of CO_2 in air) the absorption of CO_2 into the catholyte that contains $CaCO_3$ and $Mg(OH)_2$ results in progressive $Mg(OH)_2$ dissolution and the stabilization of atmospherically derived CO_2 in the form of HCO_3^- and CO_3^{2-} species; while the $CaCO_3$ that is present remains stable and unaffected. Careful analysis shows that herein all residual Ca^{2+} precipitates as $CaCO_3$, while the dissolution of $Mg(OH)_2$ in the presence of CO_2 results in the precipitation of hydromagnesite and nesquehonite according to their respective saturation states, since magnesite formation is unachievable at DIC levels (carbonate ion activities) relevant to atmospheric CO_2 conditions (see **Figure 9**). Once deployed into the ocean, the hydrated magnesium carbonates redissolve, increasing alkalinity. This analysis generally matches our experimental observations; and as a result of progressive CO_2 dissolution and stabilization, the pH of the catholyte decreases from

~12.1 to ~9.0, corresponding with the dissolution of brucite. While this "ISBL" approach requires aeration that implies an energy demand it is desirable in that it eliminates the uncertainty of CO_2 removal and allows "in plant" quantifications of both the rate and extent of CO_2 removal. The obvious disadvantage is that it implies moving large quantities of air which enhances the overall energy need of the process.

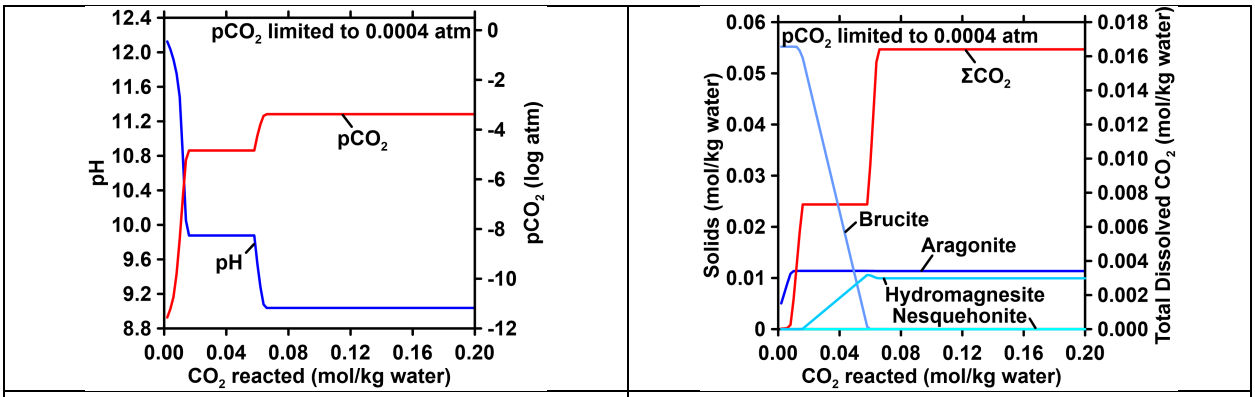

Figure 9. The changes in **(a)** pH, **(b)** solid phase assemblage, and total dissolved CO_2 in the catholyte during reaction with CO_2 to achieve equilibrium pCO_2 equivalent to atmospheric conditions at 25 °C. These simulations show that the catholyte solids discharge include hydromagnesite and aragonite, in general agreement with our experiments.

Equatic^{TM}'s Measurement, Reporting and Verification (MRV) approach for CO_2 removal

The net extent of CDR (CO_2 removal) accomplished by the *Equatic^{TM}* process must be measurable, verifiable, reportable, additional, and durable (permanent). In addition, the potential for leakage, harm, and co-benefits must be considered. Using the analysis presented in the sections above and in alignment with a recent approach suggested by CarbonPlan,[63] we can unambiguously calculate the net extent of CO_2 removal effected by the *Equatic^{TM}* process as follows:

$$\text{Total Carbon Removal}_{CO2e} = \text{Drawdown}_{CO2e} - \text{Emissions}_{CO2e}$$

where, Emissions_{CO2e} includes the total embodied CO_2 emissions from material and energy use (e.g., the grid emissions factor of electricity, and the amount of energy embodied in the co-produced hydrogen assuming typical purification demands, and conversion efficiencies), and:

$$\text{Drawdown}_{CO2e} = \text{Equatic}_{\text{Dissolved, }CO2e} + \text{Equatic}_{\text{Solid, }CO2e} - \text{Evasion from seawater}$$

The CO_2 sequestered as dissolved HCO_3^- and CO_3^{2-} ions, and solid carbonates can be quantified unambiguously by weighing the masses of $Mg(OH)_2$ and $CaCO_3$ produced, and multiplying these masses by a *carbon removal factor*, as follows (in units of g CO_2 per m^3 of water processed):

458 Equatic $_{Dissolved, CO2e}$ (g CO_2/m^3 water) = mass % $Mg(OH)_2$ × total mass of solids (g/m^3 water) × (1.7
459 mol CO_2/mol $Mg(OH)_2$) × (44.01 g CO_2/mol CO_2) × (1 mol $Mg(OH)_2$/58.3197 g
460 $Mg(OH)_2$)
461
462 Equatic $_{Solid, CO2e}$ (g CO_2/m^3 water) = mass % $CaCO_3$ × total mass of solids (g/m^3 water) × (1 mol
463 CO_2/mol $CaCO_3$) × (44.01 g CO_2/mol CO_2) × (1 mol $CaCO_3$/100.0869 g $CaCO_3$)
464
465 The total mass of the solids can be directly measured by separating the solids from the
466 catholyte effluent stream, and the mass percentages of $Mg(OH)_2$ and $CaCO_3$ quantified – online,
467 and in real-time, using thermogravimetric analysis (TGA). The carbon removal factor for Equatic
468 $_{Dissolved, CO2e}$ is affected by the extent of $Mg(OH)_2$ dissolution and the extent of CO_2 absorption
469 (into water) from air. The ISBL approach discussed above eliminates these uncertainties. The
470 evasion of CO_2 from seawater may result from secondary $CaCO_3$ precipitation or the mixing of
471 un-neutralized acid (anolyte), albeit only in the case of the "in ocean" approach, considerations
472 of which are addressed above. While there are uncertainties regarding increasing the dissolved
473 inorganic carbon (DIC) content of the oceans, notably, the *Equatic*^{TM} approach counteracts
474 ocean acidification, which has been shown to significantly, favorably, influence marine life.[64]
475
476 **SUMMARY AND CONCLUSIONS**
477 This paper presents a rigorous analysis of the *Equatic*^{TM}: ocean-mediated process for
478 carbon dioxide removal (CDR). We examine two limiting pathways for CDR, one in which CO_2 is
479 trapped solely within calcium and magnesium carbonates, and another in which CO_2 is stored
480 both as solid carbonates and as aqueous HCO_3^- and CO_3^{2-} by means of ocean alkalinity
481 enhancement promoted by $Mg(OH)_2$ dissolution. We carefully examine how the anolyte and
482 catholyte effluents of the process present unique opportunities for rock dissolution and durable
483 and permanent CO_2 immobilization. We furthermore show how the process offers flexibility to
484 eliminate the uncertainties associated with quantifying the rate and extent of CDR and also
485 minimize any detrimental changes in seawater composition and chemistry from the influent to
486 the effluent. Furthermore, detailed considerations for realkalinization of the effluent including
487 acid neutralization capacity and reactivity of diverse mineral solutes were discussed. This
488 analysis provides the fundamental basis that justifies the viability of the approach and lays the
489 foundation of a quantitative approach for MRV of the *Equatic*^{TM} process.
490
491 **Funding Sources**
492 The authors acknowledge financial support provided by: The Grantham Foundation for
493 the Protection of the Environment, the Chan Zuckerberg Initiative (CZI)/Chan Zuckerberg
494 Initiative Foundation (CZIF), the Public Utilities Board (PUB): Singapore's National Water
495 Agency, the Temasek Foundation, the National Science Foundation (NSF: Award # 2028462, and
496 CAREER Award # 2143159), the U.S. Department of Energy's Advanced Research Projects
497 Agency-Energy (ARPA-E: AMENDER: DE-AR0001551), and UCLA's Institute for Carbon
498 Management via the CAMELOT Technology Translation Initiative. The contents of this paper
499 reflect the views and opinions of the authors, who are responsible for the accuracy of the
500 datasets presented herein, and do not reflect the views and/or polices of the agency, nor do
501 the contents constitute a specification, standard or regulation. The authors acknowledge the

many individuals (too numerous to name individually) who have advised and assisted, challenged and informed, and advanced our thinking as related to ocean-based carbon dioxide removal, and the opportunities and challenges therein over the years.

REFERENCES

(1) National Academies of Sciences, Engineering, and Medicine. Negative Emissions Technologies and Reliable Sequestration: A Research Agenda, 2019.

(2) Kelemen, P. B.; McQueen, N.; Wilcox, J.; Renforth, P.; Dipple, G.; Vankeuren, A. P. Engineered Carbon Mineralization in Ultramafic Rocks for CO_2 Removal from Air: Review and New Insights. *Chem. Geol.* **2020**, *550*, 119628. https://doi.org/10.1016/j.chemgeo.2020.119628.

(3) Matter, J. M.; Stute, M.; Snæbjörnsdottir, S. Ó.; Oelkers, E. H.; Gislason, S. R.; Aradottir, E. S.; Sigfusson, B.; Gunnarsson, I.; Sigurdardottir, H.; Gunnlaugsson, E.; Axelsson, G.; Alfredsson, H. A.; Wolff-Boenisch, D.; Mesfin, K.; Taya, D. F. de la R.; Hall, J.; Dideriksen, K.; Broecker, W. S. Rapid Carbon Mineralization for Permanent Disposal of Anthropogenic Carbon Dioxide Emissions. *Science* **2016**, *352* (6291), 1312–1314. https://doi.org/10.1126/science.aad8132.

(4) La Plante, E. C.; Mehdipour, I.; Shortt, I.; Yang, K.; Simonetti, D.; Bauchy, M.; Sant, G. N. Controls on CO2 Mineralization Using Natural and Industrial Alkaline Solids under Ambient Conditions. *ACS Sustain. Chem. Eng.* **2021**, *9* (32), 10727–10739. https://doi.org/10.1021/acssuschemeng.1c00838.

(5) Veizer, J.; Hoefs, J.; Lowe, D. R.; Thurston, P. C. Geochemistry of Precambrian Carbonates: II. Archean Greenstone Belts and Archean Sea Water. *Geochim. Cosmochim. Acta* **1989**, *53* (4), 859–871. https://doi.org/10.1016/0016-7037(89)90031-8.

(6) Sundquist, E. T. Geological Perspectives on Carbon Dioxide and the Carbon Cycle. In *The Carbon Cycle and Atmospheric CO_2: Natural Variations Archean to Present*; American Geophysical Union (AGU), 1985; pp 55–59. https://doi.org/10.1029/GM032p0005.

(7) Renforth, P.; Henderson, G. Assessing Ocean Alkalinity for Carbon Sequestration. *Rev. Geophys.* **2017**, *55* (3), 636–674. https://doi.org/10.1002/2016RG000533.

(8) Ken Caldeira; Makoto Akai. Ocean Storage. In *IPCC special report on carbon dioxide capture and storage*; Cambridge: Cambridge University Press, 2005.

(9) Watson, A. J.; Schuster, U.; Shutler, J. D.; Holding, T.; Ashton, I. G. C.; Landschützer, P.; Woolf, D. K.; Goddijn-Murphy, L. Revised Estimates of Ocean-Atmosphere CO_2 Flux Are Consistent with Ocean Carbon Inventory. *Nat. Commun.* **2020**, *11* (1), 4422. https://doi.org/10.1038/s41467-020-18203-3.

(10) House, K. Z.; House, C. H.; Schrag, D. P.; Aziz, M. J. Electrochemical Acceleration of Chemical Weathering as an Energetically Feasible Approach to Mitigating Anthropogenic Climate Change. *Environ. Sci. Technol.* **2007**, *41* (24), 8464–8470. https://doi.org/10.1021/es0701816.

(11) Xie, H.; Liu, T.; Hou, Z.; Wang, Y.; Wang, J.; Tang, L.; Jiang, W.; He, Y. Using Electrochemical Process to Mineralize CO_2 and Separate Ca^{2+}/Mg^{2+} Ions from Hard Water to Produce High Value-Added Carbonates. *Environ. Earth Sci.* **2015**, *73* (11), 6881–6890. https://doi.org/10.1007/s12665-015-4401-z.

(12) Xie, H.; Liu, T.; Wang, Y.; Wu, Y.; Wang, F.; Tang, L.; Jiang, W.; Liang, B. Enhancement of Electricity Generation in CO_2 Mineralization Cell by Using Sodium Sulfate as the Reaction Medium. *Appl. Energy* **2017**, *195*, 991–999. https://doi.org/10.1016/j.apenergy.2017.03.072.

(13) Sharifian, R.; M. Wagterveld, R.; A. Digdaya, I.; Xiang, C.; A. Vermaas, D. Electrochemical Carbon Dioxide Capture to Close the Carbon Cycle. *Energy Environ. Sci.* **2021**, *14* (2), 781–814. https://doi.org/10.1039/D0EE03382K.

(14) Sharifian, R.; Boer, L.; Wagterveld, R. M.; Vermaas, D. A. Oceanic Carbon Capture through Electrochemically Induced in Situ Carbonate Mineralization Using Bipolar Membrane. *Chem. Eng. J.* **2022**, *438*, 135326. https://doi.org/10.1016/j.cej.2022.135326.

(15) La Plante, E. C.; Simonetti, D. A.; Wang, J.; Al-Turki, A.; Chen, X.; Jassby, D.; Sant, G. N. Saline Water-Based Mineralization Pathway for Gigatonne-Scale CO_2 Management. *ACS Sustain. Chem. Eng.* **2021**, *9* (3), 1073–1089. https://doi.org/10.1021/acssuschemeng.0c08561.

(16) Parkhurst, D. L.; Appelo, C. A. J. Description of Input and Examples for PHREEQC Version 3—a Computer Program for Speciation, Batch-Reaction, One-Dimensional Transport, and Inverse Geochemical Calculations. *US Geol. Surv. Tech. Methods Book* **2013**, *6*, 497.

(17) Millero, F. J.; Feistel, R.; Wright, D. G.; McDougall, T. J. The Composition of Standard Seawater and the Definition of the Reference-Composition Salinity Scale. *Deep Sea Res. Part Oceanogr. Res. Pap.* **2008**, *55* (1), 50–72. https://doi.org/10.1016/j.dsr.2007.10.001.

(18) NOAA US Department of Commerce. *Global Monitoring Laboratory - Carbon Cycle Greenhouse Gases*. https://gml.noaa.gov/ccgg/trends/mlo.html (accessed 2021-09-08).

(19) Dickson, A. G. An Exact Definition of Total Alkalinity and a Procedure for the Estimation of Alkalinity and Total Inorganic Carbon from Titration Data. *Deep Sea Res. Part Oceanogr. Res. Pap.* **1981**, *28* (6), 609–623. https://doi.org/10.1016/0198-0149(81)90121-7.

(20) Wolf-Gladrow, D. A.; Zeebe, R. E.; Klaas, C.; Körtzinger, A.; Dickson, A. G. Total Alkalinity: The Explicit Conservative Expression and Its Application to Biogeochemical Processes. *Mar. Chem.* **2007**, *106* (1), 287–300. https://doi.org/10.1016/j.marchem.2007.01.006.

(21) Middelburg, J. J.; Soetaert, K.; Hagens, M. Ocean Alkalinity, Buffering and Biogeochemical Processes. *Rev. Geophys.* **2020**, *58* (3), e2019RG000681. https://doi.org/10.1029/2019RG000681.

(22) Zeebe, R. E.; Wolf-Gladrow, D. *CO_2 in Seawater: Equilibrium, Kinetics, Isotopes*, Third Impression 2005 (with corrections).; Elsevier Science: Amsterdam ; New York, 2001.

(23) Mook, W. G. Chapter 9: Chemistry of Carbonic Acid in Water. In *Environmental Isotopes in the Hydrological Cycle: Principles and Applications*; International Atomic Energy Agency, 2001; Vol. 1, pp 87–98.

(24) Dickson, A. G. The Carbon Dioxide System in Seawater: Equilibrium Chemistry and Measurements. *Guide Best Pract. Ocean Acidif. Res. Data Report.* **2010**, *1*, 17–40.

(25) Millero, F. J.; Roy, R. N. A Chemical Equilibrium Model for the Carbonate System in Natural Waters. *Croat. Chem. Acta* **1997**, *70* (1), 1–38.

(26) Butler, J. N. *Ionic Equilibrium: Solubility and PH Calculations*; John Wiley & Sons, 1998.

(27) Hain, M. P.; Sigman, D. M.; Higgins, J. A.; Haug, G. H. The Effects of Secular Calcium and Magnesium Concentration Changes on the Thermodynamics of Seawater Acid/Base Chemistry: Implications for Eocene and Cretaceous Ocean Carbon Chemistry and

Buffering. *Glob. Biogeochem. Cycles* **2015**, *29* (5), 517–533. https://doi.org/10.1002/2014GB004986.

(28) Hänchen, M.; Prigiobbe, V.; Baciocchi, R.; Mazzotti, M. Precipitation in the Mg-Carbonate System—Effects of Temperature and CO_2 Pressure. *Chem. Eng. Sci.* **2008**, *63* (4), 1012–1028. https://doi.org/10.1016/j.ces.2007.09.052.

(29) Shaojun, Z.; Mucci, A. Calcite Precipitation in Seawater Using a Constant Addition Technique: A New Overall Reaction Kinetic Expression. *Geochim. Cosmochim. Acta* **1993**, *57* (7), 1409–1417. https://doi.org/10.1016/0016-7037(93)90002-E.

(30) Sabbides, T.; Giannimaras, E.; Koutsoukos, P. G. The Precipitation of Calcium Carbonate in Artificial Seawater at Sustained Supersaturation. *Environ. Technol.* **1992**, *13* (1), 73–80.

(31) Lin, Y.-P.; Singer, P. C.; Aiken, G. R. Inhibition of Calcite Precipitation by Natural Organic Material: Kinetics, Mechanism, and Thermodynamics. *Environ. Sci. Technol.* **2005**, *39* (17), 6420–6428. https://doi.org/10.1021/es050470z.

(32) Zuddas, P.; Mucci, A. Kinetics of Calcite Precipitation from Seawater: II. The Influence of the Ionic Strength. *Geochim. Cosmochim. Acta* **1998**, *62* (5), 757–766. https://doi.org/10.1016/S0016-7037(98)00026-X.

(33) Burton, E. A.; Walter, L. M. The Role of PH in Phosphate Inhibition of Calcite and Aragonite Precipitation Rates in Seawater. *Geochim. Cosmochim. Acta* **1990**, *54* (3), 797–808. https://doi.org/10.1016/0016-7037(90)90374-T.

(34) Bischoff, J. L. Catalysis, Inhibition, and the Calcite-Aragonite Problem; [Part] 2, The Vaterite-Aragonite Transformation. *Am. J. Sci.* **1968**, *266* (2), 80–90. https://doi.org/10.2475/ajs.266.2.80.

(35) Mucci, A.; Canuel, R.; Zhong, S. The Solubility of Calcite and Aragonite in Sulfate-Free Seawater and the Seeded Growth Kinetics and Composition of the Precipitates at 25°C. *Chem. Geol.* **1989**, *74* (3), 309–320. https://doi.org/10.1016/0009-2541(89)90040-5.

(36) Cao, L.; Caldeira, K. Atmospheric Carbon Dioxide Removal: Long-Term Consequences and Commitment. *Environ. Res. Lett.* **2010**, *5* (2), 024011. https://doi.org/10.1088/1748-9326/5/2/024011.

(37) Cohen, A. L.; McCorkle, D. C.; de Putron, S.; Gaetani, G. A.; Rose, K. A. Morphological and Compositional Changes in the Skeletons of New Coral Recruits Reared in Acidified Seawater: Insights into the Biomineralization Response to Ocean Acidification. *Geochem. Geophys. Geosystems* **2009**, *10* (7). https://doi.org/10.1029/2009GC002411.

(38) Fabry, V. J.; Seibel, B. A.; Feely, R. A.; Orr, J. C. Impacts of Ocean Acidification on Marine Fauna and Ecosystem Processes. *ICES J. Mar. Sci.* **2008**, *65* (3), 414–432. https://doi.org/10.1093/icesjms/fsn048.

(39) Milazzo, M.; Rodolfo-Metalpa, R.; Chan, V. B. S.; Fine, M.; Alessi, C.; Thiyagarajan, V.; Hall-Spencer, J. M.; Chemello, R. Ocean Acidification Impairs Vermetid Reef Recruitment. *Sci. Rep.* **2014**, *4* (1), 4189. https://doi.org/10.1038/srep04189.

(40) Segev, E.; Erez, J. Effect of Mg/Ca Ratio in Seawater on Shell Composition in Shallow Benthic Foraminifera. *Geochem. Geophys. Geosystems* **2006**, *7* (2). https://doi.org/10.1029/2005GC000969.

(41) Dilek, Y. Ophiolite Concept and Its Evolution. *Geol. Soc. Am.* **2003**. https://doi.org/10.1130/0-8137-2373-6.1.

(42) Ali, M. Y.; Watts, A. B.; Searle, M. P.; Keats, B.; Pilia, S.; Ambrose, T. Geophysical Imaging of Ophiolite Structure in the United Arab Emirates. *Nat. Commun.* **2020**, *11* (1), 2671. https://doi.org/10.1038/s41467-020-16521-0.

(43) Schuiling, R. D.; De Boer, P. L. Coastal Spreading of Olivine to Control Atmospheric CO2 Concentrations: A Critical Analysis of Viability. Comment: Nature and Laboratory Models Are Different. *Int. J. Greenh. Gas Control* **2010**, *4* (5), 855.

(44) Statista. *Global production of lime 2021*. Statista. https://www.statista.com/statistics/1006040/production-of-lime-worldwide/ (accessed 2022-07-25).

(45) Renforth, P. The Negative Emission Potential of Alkaline Materials. *Nat. Commun.* **2019**, *10* (1), 1401. https://doi.org/10.1038/s41467-019-09475-5.

(46) Latif, M. A.; Naganathan, S.; Razak, H. A.; Mustapha, K. N. Performance of Lime Kiln Dust as Cementitious Material. *Procedia Eng.* **2015**, *125*, 780–787. https://doi.org/10.1016/j.proeng.2015.11.135.

(47) *Ward's® Olivine (Fine)*. VWR. https://www.wardsci.com/store/product/8882507/ward-s-olivine-fine (accessed 2022-05-10).

(48) Kalina, L.; Bílek, V.; Kiripolský, T.; Novotný, R.; Másilko, J. Cement Kiln By-Pass Dust: An Effective Alkaline Activator for Pozzolanic Materials. *Mater. Basel Switz.* **2018**, *11* (9), E1770. https://doi.org/10.3390/ma11091770.

(49) Pokrovsky, O. S.; Schott, J. Kinetics and Mechanism of Forsterite Dissolution at 25°C and PH from 1 to 12. *Geochim. Cosmochim. Acta* **2000**, *64* (19), 3313–3325. https://doi.org/10.1016/S0016-7037(00)00434-8.

(50) Schott, J.; Pokrovsky, O. S.; Oelkers, E. H. The Link Between Mineral Dissolution/Precipitation Kinetics and Solution Chemistry. *Rev. Mineral. Geochem.* **2009**, *70* (1), 207–258. https://doi.org/10.2138/rmg.2009.70.6.

(51) Oelkers, E. H.; Schott, J. Experimental Study of Anorthite Dissolution and the Relative Mechanism of Feldspar Hydrolysis. *Geochim. Cosmochim. Acta* **1995**, *59* (24), 5039–5053. https://doi.org/10.1016/0016-7037(95)00326-6.

(52) Brantley, S. L. Kinetics of Mineral Dissolution. In *Kinetics of Water-Rock Interaction*; Brantley, S. L., Kubicki, J. D., White, A. F., Eds.; Springer New York: New York, NY, 2008; pp 151–210. https://doi.org/10.1007/978-0-387-73563-4_5.

(53) McDuff, R. E.; Morel, F. M. M. The Geochemical Control of Seawater (Sillen Revisited). *Environ. Sci. Technol.* **1980**, *14* (10), 1182–1186. https://doi.org/10.1021/es60170a007.

(54) Nguyen Dang, D.; Gascoin, S.; Zanibellato, A.; G. Da Silva, C.; Lemoine, M.; Riffault, B.; Sabot, R.; Jeannin, M.; Chateigner, D.; Gil, O. Role of Brucite Dissolution in Calcium Carbonate Precipitation from Artificial and Natural Seawaters. *Cryst. Growth Des.* **2017**, *17* (4), 1502–1513. https://doi.org/10.1021/acs.cgd.6b01305.

(55) Pokrovsky, O. S.; Schott, J. Experimental Study of Brucite Dissolution and Precipitation in Aqueous Solutions: Surface Speciation and Chemical Affinity Control. *Geochim. Cosmochim. Acta* **2004**, *68* (1), 31–45. https://doi.org/10.1016/S0016-7037(03)00238-2.

(56) Moras, C. A.; Bach, L. T.; Cyronak, T.; Joannes-Boyau, R.; Schulz, K. G. Ocean Alkalinity Enhancement - Avoiding Runaway $CaCO_3$ Precipitation during Quick and Hydrated Lime Dissolution. *Biogeosciences Discuss.* **2021**, 1–31. https://doi.org/10.5194/bg-2021-330.

(57) Zhang, H.; Menemenlis, D.; Fenty, I. ECCO LLC270 Ocean-Ice State Estimate. **2018**.

(58) He, J.; Tyka, M. D. Limits and CO_2 Equilibration of Near-Coast Alkalinity Enhancement. *EGUsphere Prepr.* **2022**, 1–26. https://doi.org/10.5194/egusphere-2022-683.
(59) Thorpe, S. A. *An Introduction to Ocean Turbulence*; Cambridge University Press: New York, 2007.
(60) Barkley, R. A. Johnston Atoll's Wake. *J. Mar. Res.* **1972**, *30* (2), 201–216.
(61) Moum, J. N. Variations in Ocean Mixing from Seconds to Years. *Annu Rev Mar Sci* **2021**, *13*, 201–226.
(62) Jones, D. C.; Ito, T.; Takano, Y.; Hsu, W.-C. Spatial and Seasonal Variability of the Air-Sea Equilibration Timescale of Carbon Dioxide. *Glob. Biogeochem. Cycles* **2014**, *28* (11), 1163–1178. https://doi.org/10.1002/2014GB004813.
(63) Chay, F.; Klitzke, J.; Hausfather, Z.; Martin, K.; Freeman, J.; Cullenward, D. *Verification Confidence Levels for Carbon Dioxide Removal*; CarbonPlan, 2022. https://carbonplan.org/research/cdr-verification-explainer.
(64) Kroeker, K. J.; Kordas, R. L.; Crim, R.; Hendriks, I. E.; Ramajo, L.; Singh, G. S.; Duarte, C. M.; Gattuso, J.-P. Impacts of Ocean Acidification on Marine Organisms: Quantifying Sensitivities and Interaction with Warming. *Glob. Change Biol.* **2013**, *19* (6), 1884–1896. https://doi.org/10.1111/gcb.12179.